ELSEVIER

Available at WWW.MATHEMATICSWEB.ORG POWERED BY SCIENCE DIRECT®

Applied Numerical Mathematics 45 (2003) 453–473

APPLIED NUMERICAL MATHEMATICS

www.elsevier.com/locate/apnum

Finite volume methods, unstructured meshes and strict stability for hyperbolic problems

Jan Nordström [a,b,*], Karl Forsberg [a], Carl Adamsson [b], Peter Eliasson [a]

[a] *Computational Aerodynamics Department, Aerodynamics Division (FFA), The Swedish Defense Research Agency (FOI), Stockholm, Sweden*

[b] *Department of Scientific Computing, Information Technology, Uppsala University, Uppsala, Sweden*

Abstract

The unstructured node centered finite volume method is analyzed and it is shown that it can be interpreted in the framework of summation by parts operators. It is also shown that introducing boundary conditions weakly produces strictly stable formulations. Numerical experiments corroborate the analysis.

1. Introduction

In computational fluid dynamics as well as computational electromagnetics, finite volume methods (FVM) formulated on unstructured grids are widely used to handle complex geometries, see, for example [31,21,8,19,18,20,14,13,28,16,15,9,7]. In [22] it was shown that strictly stable finite volume methods on structured grids can be constructed from so-called summation by parts (SBP) operators by imposing the boundary conditions weakly.

Strict stability, which means that the growth rate of the semi-discrete solution is less than or equal to the growth rate of the analytic solution, is important for long time calculations because it prevents error growth in time for realistic meshes, see [17,5,24,25,3,2,10,1,27,26,12,29,30].

The analysis in [22] relied heavily on explicit matrix manipulations enabled by the structured grid. In this work, the SBP-character of the scheme is derived directly by using Green's formula. A weak procedure to introduce boundary conditions is shown to produce energy estimates that lead to strict stability. This method is equivalent to the standard penalty procedure, called SAT (simultaneous approximation term) [6], often used for high order finite difference operators of SBP-character.

* Corresponding author.
E-mail address: nmj@ffa.se (J. Nordström).

0168-9274/03/$30.00
doi:10.1016/S0168-9274(02)00239-8

2. Analysis

The problem considered in this paper is of the form:

$$u_t + Au_x + Bu_y = 0, \quad (x, y) \in \Omega \subset \mathbb{R}^2, \tag{1}$$

with suitable boundary and initial conditions. In (1), u is the vector of unknowns and A and B are constant, symmetric, square matrices. The energy method (see for example [11]) applied to (1) gives

$$\frac{\mathrm{d}}{\mathrm{d}t}\|u\|_\Omega^2 = -\oint_{\partial\Omega} u^{\mathrm{T}} A \,\mathrm{d}y + \oint_{\partial\Omega} u^{\mathrm{T}} Bu \,\mathrm{d}x = -\oint_{\partial\Omega} u^{\mathrm{T}}\big(A\hat{x} + B\hat{y}\big)u \cdot \hat{n} \,\mathrm{d}s, \tag{2}$$

with the use of Green's formula and the symmetry of A and B. In (2), $\|u\|^2 = \iint u^2 \,\mathrm{d}x\,\mathrm{d}y$, $\hat{n}$ is the outward pointing unit normal to $\partial\Omega$, $\hat{x}$ and $\hat{y}$ are the unit vectors in the x- and y-directions and $\mathrm{d}s$ is the infinitesimal arc length element counted counter clockwise around Ω.

The number of boundary conditions at any point on the boundary is the least number that make $(A\hat{x} + B\hat{y}) \cdot \hat{n}$ positive semi definite. When referring to the problem (1), it is assumed that the boundary conditions are such that this is true. In the examples in Section 3 this will be explicitly shown to hold.

2.1. SBP operators

The problem (1) is discretized in space by introducing the vector $\boldsymbol{u}$ of length $N = ln$ where l is the number of unknowns in (1) and n is the number of grid-points. The elements of $\boldsymbol{u}$ are organized such that the first n elements are the discretization of the first variable in u, the elements $n+1, \ldots, 2n$ are the discretization of the second variable and so on. Furthermore we introduce discrete operators D_x and D_y. Eq. (1) can now formally be written

$$\boldsymbol{u}_t + (A \otimes D_x)\boldsymbol{u} + (B \otimes D_y)\boldsymbol{u} = 0, \tag{3}$$

where $\otimes$ is the Kronecker product.

For 2D-equations on unstructured grids, a generalized SBP-concept will be used. We aim for Q_x and Q_y to be such that

$$\boldsymbol{\phi}^{\mathrm{T}}\big(Q_x + Q_x^{\mathrm{T}}\big)\boldsymbol{\phi} \approx \oint_{\partial\Omega} \phi^2 \,\mathrm{d}y, \qquad \boldsymbol{\phi}^{\mathrm{T}}\big(Q_y + Q_y^{\mathrm{T}}\big)\boldsymbol{\phi} \approx -\oint_{\partial\Omega} \phi^2 \,\mathrm{d}x, \tag{4}$$

where the difference operators are of the form $D_x = P^{-1}Q_x$, $D_y = P^{-1}Q_y$ and $\phi(x, y)$ is a smooth continuous function. If (4) holds, the discrete energy method applied to (3) will lead to an approximation that corresponds to Eq. (2).

2.1.1. The node-centered finite volume method

In a node centered FVM on an unstructured grid, the unknowns are associated with the nodes in the grid. The control-volumes that constitute the dual grid are defined as follows. Each control-volume is a polygon with its vertices at the centers of gravity of the surrounding triangles (or quadrilaterals) and at the midpoints of the grid-sides, see Fig. 1.

Integration of $u_t + u_x = 0$ over a control volume, Ω_C, leads to

$$\iint_{\Omega_C} u_t \,\mathrm{d}x\,\mathrm{d}y + \iint_{\Omega_C} u_x \,\mathrm{d}x\,\mathrm{d}y = \iint_{\Omega_C} u_t \,\mathrm{d}x\,\mathrm{d}y + \oint_{\partial\Omega_C} u \,\mathrm{d}y = 0. \tag{5}$$

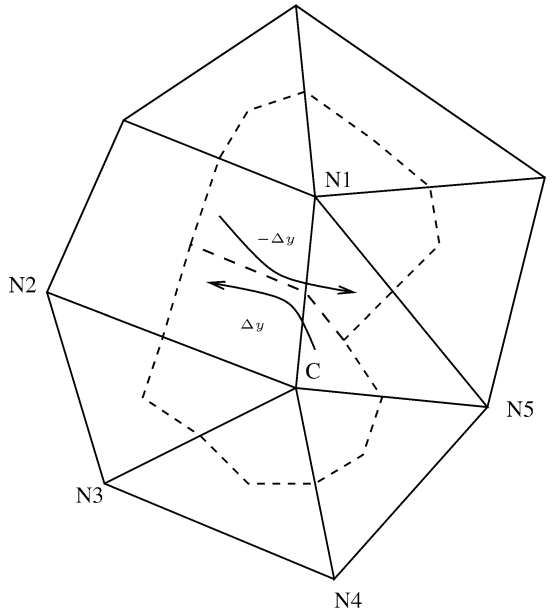

Fig. 1. Part of the grid (solid line) and the dual grid (dashed line).

A semi discrete approximation of Eq. (5) can be written

$$P\boldsymbol{u}_t + Q_x\boldsymbol{u} = 0, \tag{6}$$

where P is a diagonal matrix with the control volumes on the diagonal and Q_x associates with each node an approximation of the line integral of u around the boundary of the control volume. The approximation of this line integral, the flux, is computed as follows.

Consider a node in the interior of the mesh with index C. The flux is the integral

$$\text{flux} = \oint_{\partial\Omega_C} u\,\mathrm{d}y,$$

where Ω_C is the dual grid cell that belongs to the node C. The node C has neighbors with indices N_i, see Fig. 1. Each neighbor can be associated in a one-to-one manner with the two sides of the polygon $\partial\Omega_C$ that have a common vertex at the side connecting the neighbor to the node C. Each neighbor will contribute to the flux with one term. This term is the mean value of u_C and u_{N_i} times Δy over the corresponding dual grid side. This can formally be written:

$$\text{flux} = \sum_i \frac{u_C + u_{N_i}}{2}\Delta y_i = \sum_i u_C\frac{\Delta y_i}{2} + \sum_i u_{N_i}\frac{\Delta y_i}{2}, \tag{7}$$

where the sum goes over all neighbors to the point C. Not considering the boundary of the domain, (7) leads to

$$Q_{CC} = \sum_i \frac{\Delta y_i}{2} = 0, \qquad Q_{CN_i} = \frac{\Delta y_i}{2} = -Q_{N_iC}, \tag{8}$$

i.e., the matrix Q is skew symmetric in the interior.

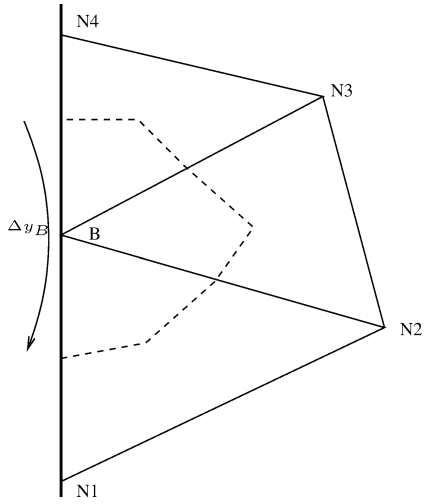

Fig. 2. The geometry at the boundary.

Let us consider the case where no boundary condition (b.c) is necessary. The flux through the boundary edge is calculated as the node value at the boundary node, u_B, times the corresponding Δy_B, see Fig. 2. Formally:

$$\text{flux} = \sum_i \frac{u_B + u_{N_i}}{2} \Delta y_i + u_B \Delta y_B = u_B \Delta y_B + \sum_i u_B \frac{\Delta y_i}{2} + \sum_i \frac{u_{N_i}}{2} \Delta y_i.$$

Note that sums are not over a closed loop. From Fig. 2 we obtain

$$\sum_i \Delta y_i = -\Delta y_B. \tag{9}$$

Thus we have

$$\text{flux} = \sum_i u_{N_i} \frac{\Delta y_i}{2} + u_B \frac{\Delta y_B}{2},$$

which leads to

$$Q_{BB} = \frac{\Delta y_B}{2}, \qquad Q_{BN_i} = \frac{\Delta y_i}{2} = -Q_{N_i B}. \tag{10}$$

Remark. The specific flux approximation (7) discussed in this section leads to a skew symmetric Q in the interior. Other types of flux approximations (involving more nodes) are of course possible. However, unless the resulting matrix is skew symmetric, instabilities might occur.

Let us now consider the case with b.c, $u = g$ at the boundary. Even though we know the u-values at the boundary a priori from the b.c we do *not* remove those points from the scheme. Instead we impose the b.c weakly. The fluxes, using (9), become:

$$\text{flux} = \sum_i \frac{u_B + u_{N_i}}{2} \Delta y_i + g_B \Delta y_B = \sum_i u_{N_i} \frac{\Delta y_i}{2} + u_B \frac{\Delta y_B}{2} + b,$$

where

$$b = \begin{cases} (g_B - u_B)\Delta y_B & \text{at the boundary with b.c,} \\ 0 & \text{otherwise.} \end{cases} \tag{11}$$

The results (8), (10) and (11) yield

$$P\boldsymbol{u}_t + Q\boldsymbol{u} + b = 0. \tag{12}$$

Remark. There is a standard penalty procedure to introduce b.c in a stable way when working with SBP-operators called SAT, see for example [6]. In the present case, when the matrix P is diagonal, the SAT procedure is equivalent to the weak procedure described above.

2.1.2. Generalization to the full problem

The generalization of (12) is straightforward. In (3) we use $D_x = P^{-1}Q_x$ and $D_y = P^{-1}Q_y$ where P, Q_x and Q_y are derived as in the previous section. The generalization of (12) becomes

$$(I \otimes P)\boldsymbol{u}_t + (A \otimes Q_x)\boldsymbol{u} + (B \otimes Q_y)\boldsymbol{u} + b = 0, \tag{13}$$

where b is a vector of the same length as $\boldsymbol{u}$, i.e., of length $N = nl$ where l is the number of unknowns and n is the number of grid points. ($\boldsymbol{u}$ is organized as in Section 2.1.) The energy method applied to (13) with $b = 0$ gives

$$\frac{\mathrm{d}}{\mathrm{d}t}\|\boldsymbol{u}\|^2_{I\otimes P} = -\boldsymbol{u}^{\mathrm{T}}\big(A \otimes \big(Q_x + Q_x^{\mathrm{T}}\big)\big)\boldsymbol{u} - \boldsymbol{u}^{\mathrm{T}}\big(B \otimes \big(Q_y + Q_y^{\mathrm{T}}\big)\big)\boldsymbol{u}^{\mathrm{T}}, \tag{14}$$

where the symmetry of A and B has been used. I is the $d \times d$ identity matrix. Note that the energy rate depends only on the symmetric part of Q_x and Q_y.

The result of Section 2.1.1 can be summarized as

$$Q_x + Q_x^{\mathrm{T}} = Y, \qquad Q_y + Q_y^{\mathrm{T}} = X, \tag{15}$$

where the non-zero elements in Y, X are Δy_i, $-\Delta x_i$, respectively. The m non-zero elements correspond to the m boundary points. The relation (15) yield

$$\boldsymbol{\phi}^{\mathrm{T}} Y \boldsymbol{\phi} = \sum_{i=1}^{m} \phi_i^2 \Delta y_i, \qquad \boldsymbol{\phi}^{\mathrm{T}} X \boldsymbol{\phi} = -\sum_{i=1}^{m} \phi_i^2 \Delta x_i, \tag{16}$$

which means that (4) holds. The introduction of (15) into (14) leads to

$$\frac{\mathrm{d}}{\mathrm{d}t}\|\boldsymbol{u}\|^2_{I\otimes P} = -\sum_{\partial\Omega} \big[\boldsymbol{u}^{\mathrm{T}}\big(A\hat{x} + B\hat{y}\big)\boldsymbol{u} \cdot \hat{n}\big]_i \Delta s_i, \tag{17}$$

where $\hat{n}_i = (\Delta y_i, -\Delta x_i)^{\mathrm{T}}/\Delta s_i$, $\Delta s_i = \sqrt{\Delta x_i^2 + \Delta y_i^2}$. We have also introduced the notation $[\boldsymbol{u}]_i = \boldsymbol{u}_i = (u_1, u_2, \ldots, u_l)_i^{\mathrm{T}}$ and $\sum_{\partial\Omega} = \sum_{i\in\partial\Omega}$. Note that the discrete estimate (17) naturally correspond to (2).

The introduction of boundary data must lead to an energy estimate. With boundary conditions in the form $u = g$ we use the boundary data to calculate the flux as described above in Section 2.1.1. If a combination of boundary data and local values are used to calculate the flux we substitute boundary data for the ingoing characteristic variables and use local data for the outgoing ones. This method is illustrated in the examples below.

2.2. Observations

The FVM discussed here can be shown to be equivalent to a finite element method (FEM) in the interior of the grid if the grid consist of triangles only. The FEM is a modification of the classical variant obtained by using piece-wise linear 'tent-functions'. The FEM can be written in the form (6) where

$$P_{ij} = \int_{\Omega} \phi_i \phi_j \,\mathrm{d}x\,\mathrm{d}y, \qquad Q_{ij} = \int_{\Omega} \phi_i \frac{\partial}{\partial x} \phi_j \,\mathrm{d}x\,\mathrm{d}y. \tag{18}$$

Here ϕ_i is the piece-wise linear function that is 1 in node i and 0 in all other nodes. The Q-matrix above can be shown to be identical to the Q-matrix from the FVM if only triangles are used. To make also the P-matrix identical, the FEM has to be lumped, i.e., the P in (18) must be changed to $P^l_{ij} = \delta_{ij} \sum_k P_{ik}$ (where δ_{ij} is the Kronecker δ-symbol).

2.3. Strict stability

Following the outline in [22] we will introduce a definition of strict stability that corresponds well with our examples below. Consider the problem (1) augmented with boundary conditions of the form

$$Lu = g, \quad (x, y) \in \partial\Omega. \tag{19}$$

In (19), L is a $d \times l$ matrix where d is the number of boundary conditions and l the number of unknowns. The energy rate (2) can be rewritten as

$$\frac{\mathrm{d}}{\mathrm{d}t}\|u\|^2 = -\oint_{\partial\Omega} \left[v^{\mathrm{T}} \Lambda^+ v + g^{\mathrm{T}} \Lambda^- g\right] \mathrm{d}s, \tag{20}$$

by specifying the d ingoing characteristic variables at the boundary $\partial\Omega$. To arrive at (20) we have used the notations

$$\left(A\hat{x} + B\hat{y}\right) \cdot \hat{n} = X \Lambda X^{\mathrm{T}}, \qquad v = X^{\mathrm{T}} u, \qquad \Lambda = \mathrm{diag}(\lambda_j) = \Lambda^+ + \Lambda^-, \tag{21}$$

where $\hat{n} = (\mathrm{d}y, -\mathrm{d}x)^{\mathrm{T}}/\mathrm{d}s$, $\mathrm{d}s = \sqrt{\mathrm{d}x^2 + \mathrm{d}y^2}$ and v are the characteristic variables. The diagonal matrix Λ with d purely negative entries is divided into Λ^+ (with zeros injected on the positions for the d purely negative entries) and Λ^- (with zeros injected on the positions for the $l - d$ non-negative entries). The boundary operator L in (19) consist of the d rows in X^{T} that correspond to the d negative eigenvalues.

The discrete approximation of (1) augmented with boundary conditions in penalty form is given by (13). The discrete energy rate is given by (17) augmented with the term $2u^{\mathrm{T}}b$. Transformation of the energy rate using the discrete version of (21) yields

$$\frac{\mathrm{d}}{\mathrm{d}t}\|\boldsymbol{u}\|^2_{I\otimes P} = -\sum_{\partial\Omega} \left[\boldsymbol{v}^{\mathrm{T}} \Lambda^+ \boldsymbol{v} + \boldsymbol{v}^{\mathrm{T}} \Lambda^- \boldsymbol{v} + 2\boldsymbol{v}^{\mathrm{T}} \Sigma(\boldsymbol{v} - g)\right]_i \Delta s_i, \tag{22}$$

where the matrix Σ_i remains to be determined. The choice $\Sigma_i = -\delta \Lambda^-_i/2$, $\delta > 0$ leads to

$$\frac{\mathrm{d}}{\mathrm{d}t}\|\boldsymbol{u}\|^2_{I\otimes P} = -\sum_{\partial\Omega} \left[\boldsymbol{v}^{\mathrm{T}} \Lambda^+ \boldsymbol{v} + g^{\mathrm{T}} \Lambda^- g\right]_i \Delta s_i + R, \tag{23}$$

where $R = \sum_{\partial\Omega} [(\delta - 1)\boldsymbol{v}^{\mathrm{T}} \Lambda^- \boldsymbol{v} + g^{\mathrm{T}} \Lambda^- g - \delta \boldsymbol{v}^{\mathrm{T}} \Lambda^- g]_i \Delta s_i$. We need the following definition.

Definition 1. Consider the estimates (20) and (23). The discrete approximation (13) of the problem (1), (19) is strictly stable if R is non-positive.

Remark. With $g \neq 0$, a strictly stable method is obtained with $\delta = 2$ which yields $R = \sum_{\partial\Omega}[(\boldsymbol{v} - g)^{\mathrm{T}} \Lambda^{-}(\boldsymbol{v} - g)]_i \Delta s_i \leqslant 0$. With $g = 0$, strict stability is obtained with $\delta \geqslant 1$. Definition 1 fits the constant coefficient problems well. However, there are other definitions of strict stability (see, for example, [11]) more suitable for general types of problems.

Remark. The penalty term in (13) for the boundary condition (19) becomes in this case

$$b_i = X_i \Sigma_i (X_i^{\mathrm{T}} u_i - g_i), \quad (x, y)_i \in \partial\Omega.$$

3. Examples

3.1. A one-dimensional linear system

The domain of computation will be $\Omega \subset \mathbb{R}^2$. The boundary of Ω will be denoted $\partial\Omega$. Define Γ_1 and Γ_2 to be such that $\Gamma_1 \cup \Gamma_2 = \partial\Omega$ and Γ_1 is the part of $\partial\Omega$ where $\hat{x} \cdot \hat{n} < 0$ where $\hat{n}$ is the outward pointing unit normal to $\partial\Omega$. This of course implies that $\hat{x} \cdot \hat{n} > 0$ on Γ_2. Moreover if $\mathrm{d}l = (\mathrm{d}x, \mathrm{d}y)$ is the infinitesimal tangent vector to $\partial\Omega$ counted counter clockwise around Ω we have that $\mathrm{d}y < 0$ on Γ_1 and $\mathrm{d}y > 0$ on Γ_2.

Consider the 1D Maxwell equations

$$\begin{pmatrix} E \\ H \end{pmatrix}_t + \begin{pmatrix} 0 & 1 \\ 1 & 0 \end{pmatrix} \begin{pmatrix} E \\ H \end{pmatrix}_x = 0, \quad (x, y) \in \Omega \subset \mathbb{R}^2, \ E|_{\partial\Omega} = 0. \tag{24}$$

The problem (24) could also be considered to be a model problem for the Euler equations. It is a very sensitive problem since

$$\frac{\mathrm{d}}{\mathrm{d}t} \iint_{\Omega} E^2 + H^2 \,\mathrm{d}x \,\mathrm{d}y = -\oint_{\partial\Omega} 2EH \,\mathrm{d}y = 0,$$

i.e., there is absolutely no dissipation present.

Let $\boldsymbol{E}$ and $\boldsymbol{H}$ denote the discrete representations of the unknowns E and H. The discrete approximation of (24) becomes,

$$\begin{pmatrix} P & 0 \\ 0 & P \end{pmatrix} \begin{pmatrix} \boldsymbol{E} \\ \boldsymbol{H} \end{pmatrix}_t + \begin{pmatrix} 0 & Q \\ Q & 0 \end{pmatrix} \begin{pmatrix} \boldsymbol{E} \\ \boldsymbol{H} \end{pmatrix} + b = 0, \tag{25}$$

where

$$b = -(\sigma_1, \sigma_2)^{\mathrm{T}} \otimes \boldsymbol{E}\boldsymbol{\Delta}\boldsymbol{y}, \qquad [\boldsymbol{E}\boldsymbol{\Delta}\boldsymbol{y}]_i = E_i \Delta y_i, \tag{26}$$

at all boundary points. The discrete energy rate becomes

$$\frac{\mathrm{d}}{\mathrm{d}t}\left(\|\boldsymbol{E}\|_P^2 + \|\boldsymbol{H}\|_P^2\right) = -2\sum_{\delta\Omega}\left[E_i H_i (1 - \sigma_2) + \sigma_1 E_i^2\right]\Delta y_i.$$

This means that the discrete energy rate corresponds exactly to the continuous case, i.e, $R = 0$ for $\sigma_1 = 0,\ \sigma_2 = 1$ and the approximation is strictly stable, see Definition 1.

Let us consider the characteristic b.c

$$(E + H)|_{\Gamma_1} = f, \qquad (E - H)|_{\Gamma_2} = g. \tag{27}$$

The energy equation (2) can, after some algebra, be written

$$\frac{\mathrm{d}}{\mathrm{d}t}\big(\|E\|^2 + \|H\|^2\big) = -\frac{1}{2}\oint_{\Gamma_1} f^2 - (E - H)^2\,\mathrm{d}y - \frac{1}{2}\oint_{\Gamma_2} (E + H)^2 - g^2\,\mathrm{d}y, \tag{28}$$

where the definitions of Γ_1 and Γ_2 show that we have an energy estimate. With the new boundary conditions (27) we need to determine b in (25).

We make the ansatz

$$\begin{aligned} b_1 &= \begin{pmatrix} \sigma_1 \\ \sigma_2 \end{pmatrix} \otimes \big((\boldsymbol{E} + \boldsymbol{H}) - \boldsymbol{f}\big)\boldsymbol{\Delta y}, \\ b_2 &= \begin{pmatrix} \sigma_3 \\ \sigma_4 \end{pmatrix} \otimes \big((\boldsymbol{E} - \boldsymbol{H}) - \boldsymbol{g}\big)\boldsymbol{\Delta y}, \end{aligned} \tag{29}$$

where subscripts $1, 2$ on b refer to Γ_1, Γ_2, respectively. In (29), the same notation as in (26) has been used.

The energy method applied to (25) with b defined in (29) leads to

$$\begin{aligned} &\frac{\mathrm{d}}{\mathrm{d}t}\big(\|\boldsymbol{E}\|_P + \|\boldsymbol{H}\|_P\big) \\ &\quad = -\frac{1}{2}\sum_{\Gamma_1}\big[\big(f_i^2 - (E_i - H_i)^2\big)\big]\Delta y_i - \frac{1}{2}\sum_{\Gamma_2}\big[\big((E_i + H_i)^2 - g_i^2\big)\big]\Delta y_i + R, \end{aligned} \tag{30}$$

where

$$R = \frac{1}{2}\sum_{\Gamma_1}\big[\big(f_i - (E_i + H_i)\big)^2\big]\Delta y_i - \frac{1}{2}\sum_{\Gamma_2}\big[\big((E_i - H_i) - g_i\big)^2\big]\Delta y_i.$$

The estimate (30) is obtained using $\sigma_1 = \sigma_2 = \sigma_4 = -1/2$ and $\sigma_3 = 1/2$.

The estimate (30) is completely similar to the continuous energy estimate (28). The definitions of Γ_1 and Γ_2 show that (30) leads to an energy estimate and that $R \leqslant 0$. The approximation (25), (29) of (24) and (27) is strictly stable in the sense of Definition 1.

The diagonal form of (24) reads

$$\begin{pmatrix} \mu \\ \nu \end{pmatrix}_t + \begin{pmatrix} 1 & 0 \\ 0 & -1 \end{pmatrix}\begin{pmatrix} \mu \\ \nu \end{pmatrix}_x = 0, \quad (x, y) \in \Omega \subset \mathbb{R}^2,\ (\mu - \nu)|_{\partial\Omega} = 0, \tag{31}$$

where $\mu = (E + H)/\sqrt{2}$, $\nu = (-E + H)/\sqrt{2}$. The energy rate becomes

$$\frac{\mathrm{d}}{\mathrm{d}t}\iint_{\Omega} \mu^2 + \nu^2\,\mathrm{d}x\,\mathrm{d}y = -\oint_{\partial\Omega} \mu^2 - \nu^2\,\mathrm{d}y = 0.$$

The discrete approximation of (31) is

$$\begin{pmatrix} P & 0 \\ 0 & P \end{pmatrix}\begin{pmatrix} \boldsymbol{\mu} \\ \boldsymbol{\nu} \end{pmatrix}_t + \begin{pmatrix} Q & 0 \\ 0 & -Q \end{pmatrix}\begin{pmatrix} \boldsymbol{\mu} \\ \boldsymbol{\nu} \end{pmatrix} + b = 0. \tag{32}$$

The ansatz

$$b = (\sigma_1, \sigma_2)^{\mathrm{T}} \otimes (\boldsymbol{v} - \boldsymbol{\mu})\boldsymbol{\Delta y}, \tag{33}$$

and the energy method applied to (32) leads to

$$\frac{\mathrm{d}}{\mathrm{d}t}\big(\|\boldsymbol{\mu}\|_P^2 + \|\boldsymbol{v}\|_P^2\big) = -\sum_{\delta\Omega}\big[(\mu_i - v_i)^2 + 2(v_i - \mu_i)(\sigma_1\mu_i + \sigma_2 v_i)\big]\Delta y_i. \tag{34}$$

By letting

$$\sigma_1 = 1, \quad \sigma_2 = 0 \quad \text{on } \Gamma_1 \quad \text{and} \quad \sigma_1 = 0, \quad \sigma_2 = 1 \quad \text{on } \Gamma_2 \tag{35}$$

we prescribe the ingoing characteristic variable and the estimate becomes,

$$\frac{\mathrm{d}}{\mathrm{d}t}\big(\|\boldsymbol{\mu}\|_P^2 + \|\boldsymbol{v}\|_P^2\big) = R = \sum_{\Gamma_1}(\mu_i - v_i)^2\Delta y_i - \sum_{\Gamma_2}(\mu_i - v_i)^2\Delta y_i.$$

Strict stability is obtained in the sense of Definition 1 since $R \leqslant 0$.

One could also update all boundary points in the same way using

$$\sigma_1 = 1/2, \quad \sigma_2 = 1/2 \quad \text{on } \delta\Omega. \tag{36}$$

This would lead to

$$\frac{\mathrm{d}}{\mathrm{d}t}\big(\|\boldsymbol{\mu}\|_P^2 + \|\boldsymbol{v}\|_P^2\big) = 0. \tag{37}$$

The discrete energy rate now correspond exactly to the continuous one ($R = 0$) and consequently strict stability is obtained.

There are other methods to introduce b.c than the weak method described above. One can, for example, remove the boundary points from the scheme altogether and satisfy the b.c exactly. This boundary procedure (called injection or strong imposition) reduces the size of the system (12), but sometimes introduces stability problems, see [22,5].

In the method of injection, the μ-points on Γ_1 and the v-points on Γ_2 are removed from the system and v is injected on Γ_1 and μ on Γ_2. This gives

$$\begin{aligned}
&\frac{\mathrm{d}}{\mathrm{d}t}\big(\|\boldsymbol{\mu}'\|_{P'}^2 + \|\boldsymbol{v}'\|_{P'}^2\big) \\
&\quad = -\begin{pmatrix}\boldsymbol{\mu}'^{\mathrm{T}} & \boldsymbol{v}'^{\mathrm{T}}\end{pmatrix}\begin{pmatrix} Q' & 0 \\ 0 & -Q'\end{pmatrix}\begin{pmatrix}\boldsymbol{\mu}' \\ \boldsymbol{v}'\end{pmatrix} + 2\begin{pmatrix}\boldsymbol{\mu}'^{\mathrm{T}} & \boldsymbol{v}'^{T}\end{pmatrix}b \\
&\quad = -\sum_{\Gamma_2}\mu_i^2\Delta y_i + \sum_{\Gamma_1} v_i^2\Delta y_i - \sum_{\widetilde{\Gamma_2}}\mu_i v_{i'}\Delta y_i + \sum_{\widetilde{\Gamma_1}} v_i\mu_{i'}\Delta y_i,
\end{aligned} \tag{38}$$

where $\widetilde{\Gamma_1}$ and $\widetilde{\Gamma_2}$ are the sets of points that are neighbors to the points in Γ_1 and Γ_2, respectively, and i' is the index of the node on the boundary that is a neighbor to the node with index i (if such a node exists). $\boldsymbol{\mu}'$, $\boldsymbol{v}'$, P' and Q'_f are the vectors and matrices where the points mentioned above are removed. The energy rate contains indefinite cross-terms which means that we cannot show strict stability in the sense of Definition 1.

3.1.1. The spectrum and the long time behavior

It can be shown that the spectrum of the continuous problem (31) consists of the points $0, \pm\pi i$, $\pm 2\pi i, \ldots$. The long time behavior of a numerical method is determined by the eigenvalues (the spectrum) of the spatial operator (including the boundary procedure). A strictly stable scheme (see Definition 1) is guaranteed to have a time growth that is less then the time growth for the continuous problem. This is an especially important aspect on the irregular coarse grids one encounter in real life calculations.

We will consider the spectrum of the methods discussed above on a fine grid with 169 nodes with almost equally sized volumes (see Fig. 10) and on a coarse irregular grid with 23 nodes (see Fig. 6). The spectrum of the spatial operators using injection, the boundary procedure (33), (35) and (36) on the fine mesh are shown in Figs. 3, 4 and 5, respectively. For all these methods, the spectrum lies in the right half plane which implies non-growing solutions. Note that the spectrum using (36) is purely imaginary which is consistent with (37).

On the coarse irregular mesh, the spectrum for the spatial operators using injection, the boundary procedure (33), (35) and (36) are shown in Figs. 7, 8 and 9 respectively. The injection method produce eigenvalues with negative real parts. These eigenvalues will lead to exponential time growth and consequently an unstable scheme. The spectrum for the strictly stable methods using penalty of the form (35) and (36) are still located in the right half of the complex plane.

3.1.2. Accuracy

The discrete spectra should converge to the continuous spectrum $(0, \pm\pi i, \pm 2\pi i, \ldots)$ when the number of nodes in the mesh increases. To investigate this, the unit square was discretized as in Fig. 10 and the smallest distance to the points πi and $2\pi i$ was plotted against the number of nodes, see Figs. 11–14.

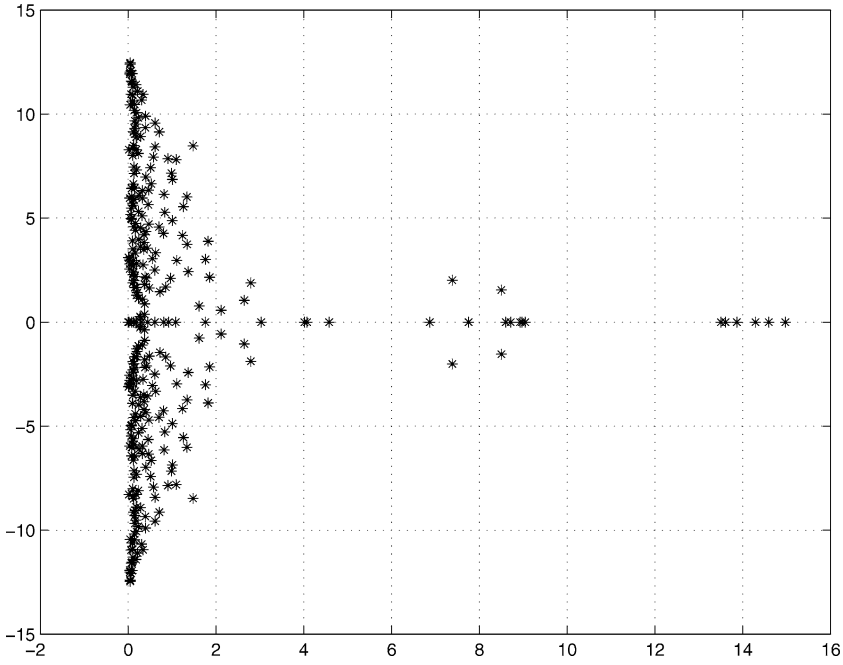

Fig. 3. The spectrum for injection on a mesh with 169 nodes. $\min(\mathrm{Re}(\lambda_i)) = 0$.

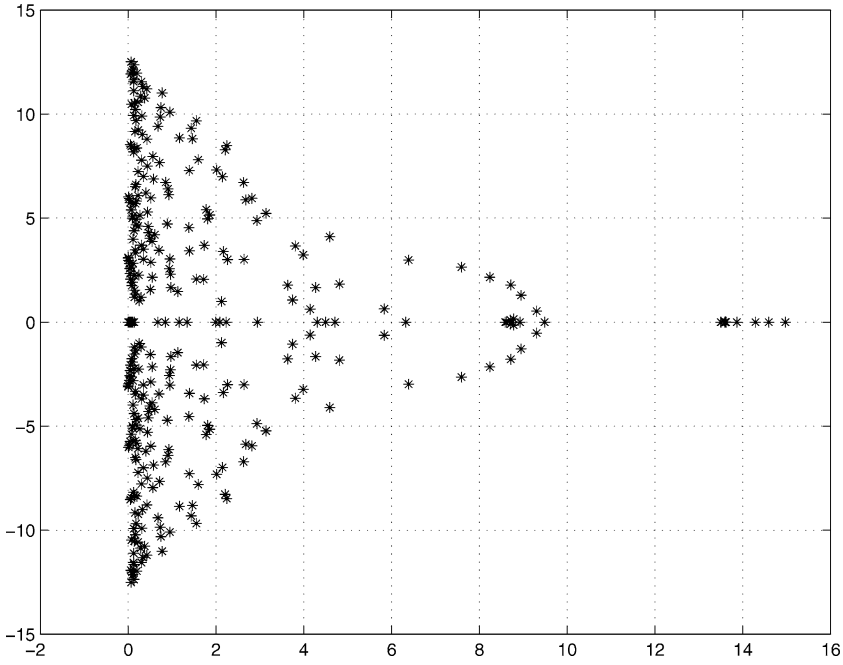

Fig. 4. The spectrum of the method defined by (35) on a mesh with 169 nodes. $\min(\mathrm{Re}(\lambda_i)) = 0$.

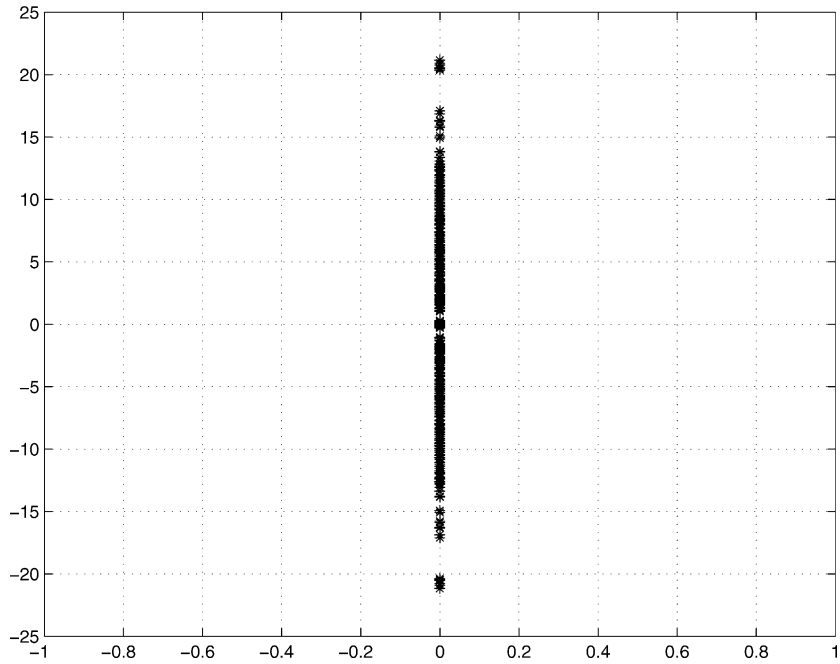

Fig. 5. The spectrum of the method defined by (36) on a mesh with 169 nodes. $\min(\mathrm{Re}(\lambda_i)) = 0$.

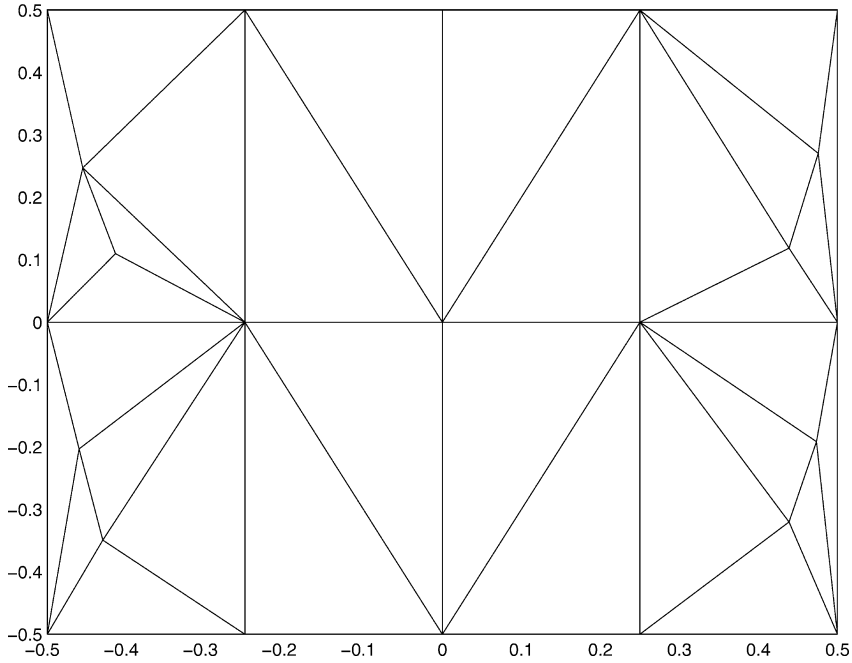

Fig. 6. A highly irregular mesh with 23 nodes.

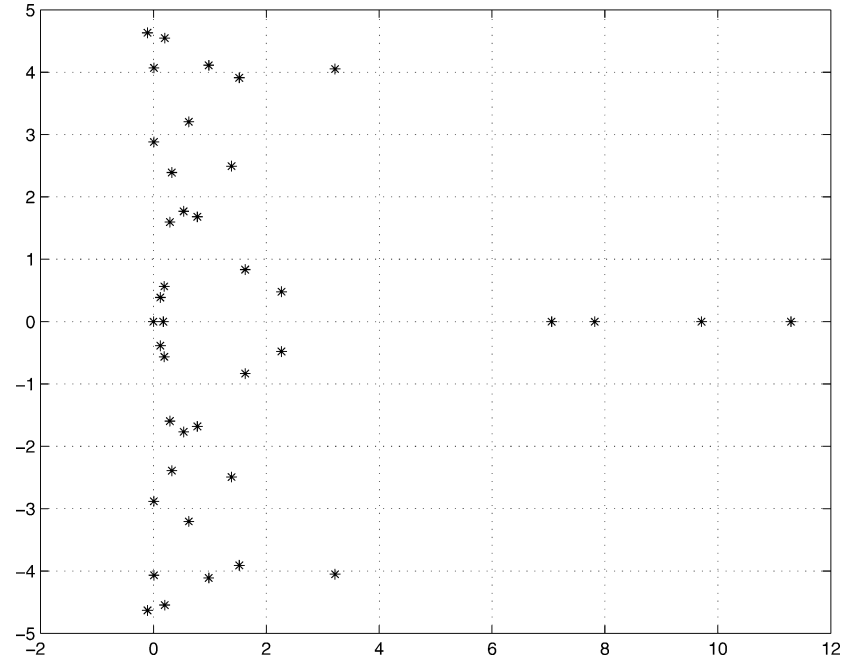

Fig. 7. The spectrum for injection on a mesh with 23 nodes. $\min(\mathrm{Re}(\lambda_i)) = -0.105$.

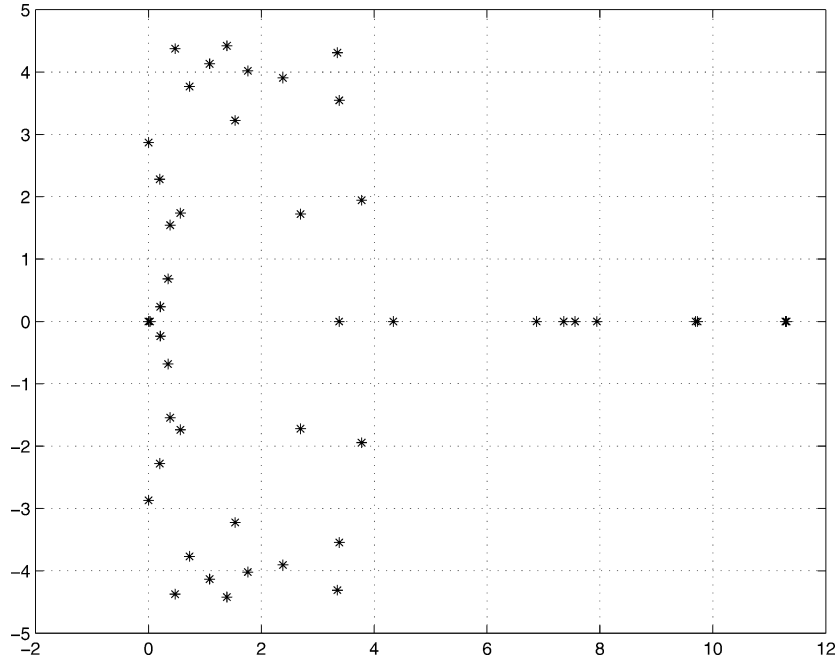

Fig. 8. The spectrum of the method defined by (35) on a mesh with 23 nodes. $\min(\mathrm{Re}(\lambda_i)) = 0$.

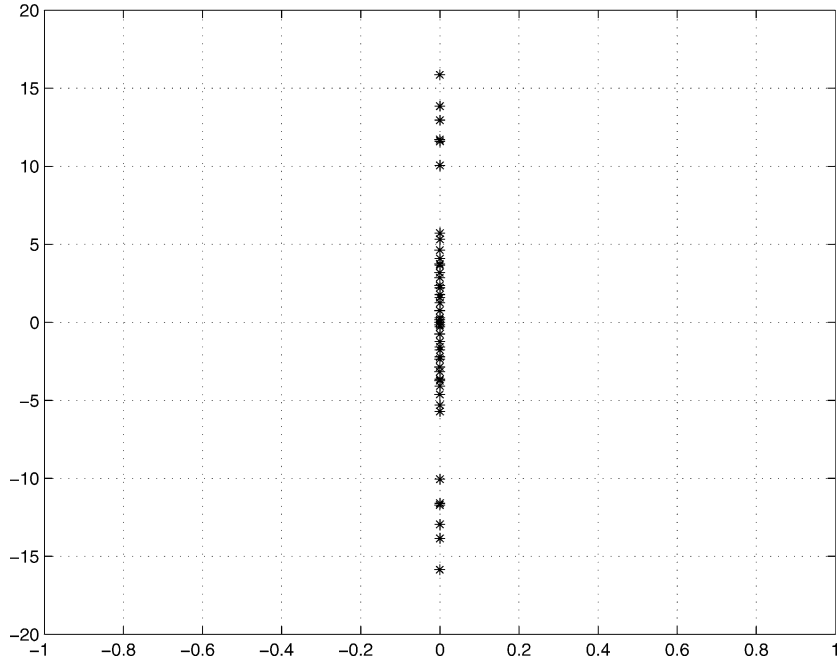

Fig. 9. The spectrum for the method defined by (36), on a mesh with 23 nodes. $\min(\mathrm{Re}(\lambda_i)) = 0$.

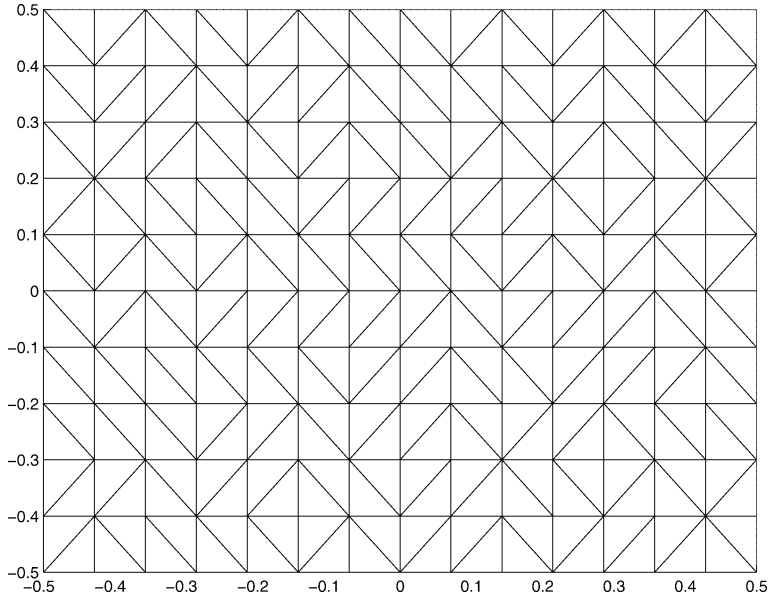

Fig. 10. A mesh with almost equally sized volumes.

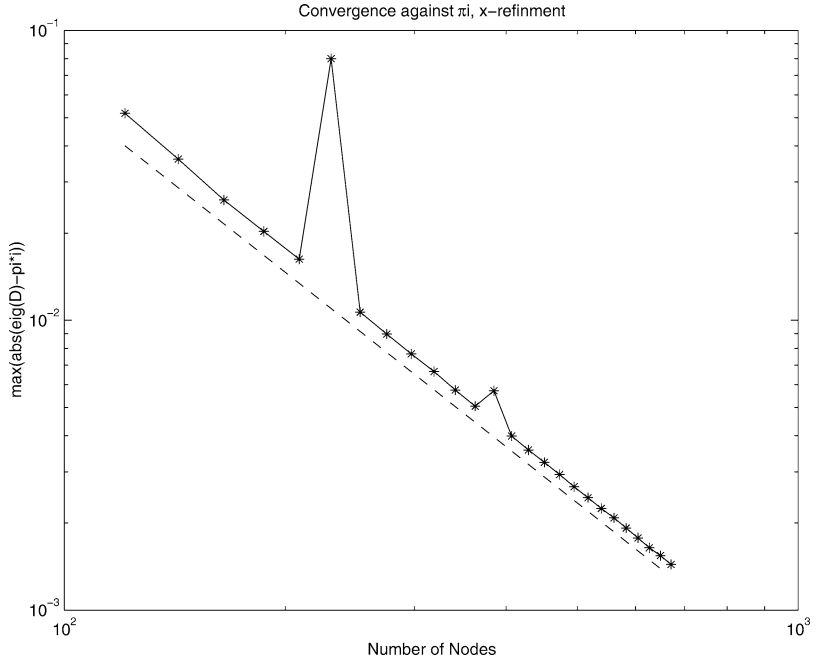

Fig. 11. Convergence against the point πi. New nodes are introduced in the x-direction only. The dashed line is a reference line with slope-2.

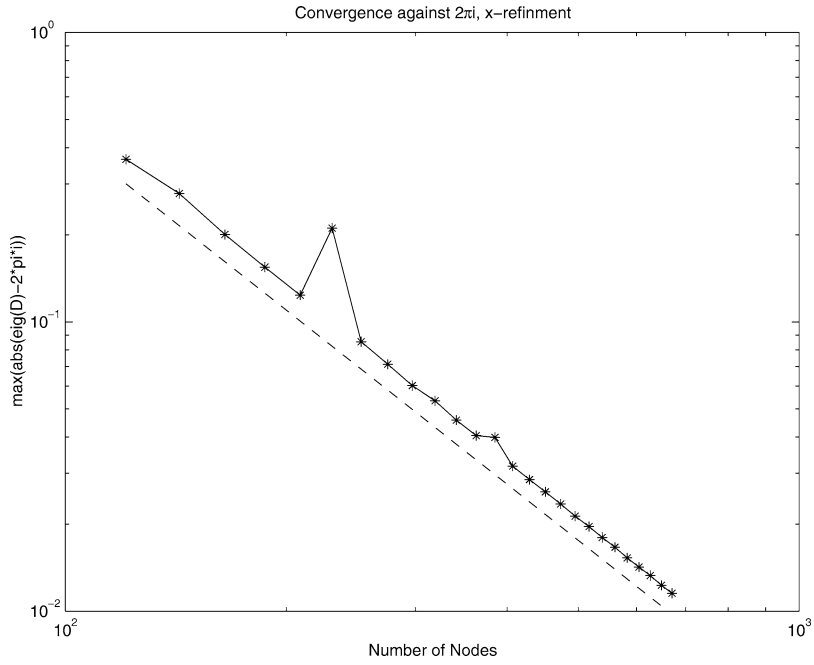

Fig. 12. Convergence against the point $2\pi i$. New nodes are introduced in the x-direction only. The dashed line is a reference line with slope-2.

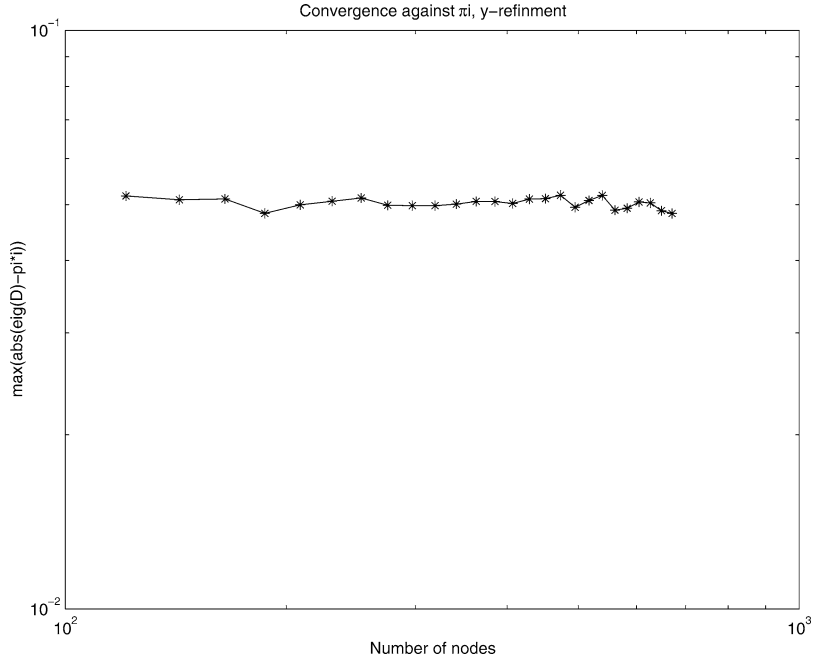

Fig. 13. Convergence against the point πi. New nodes are introduced in the y-direction only.

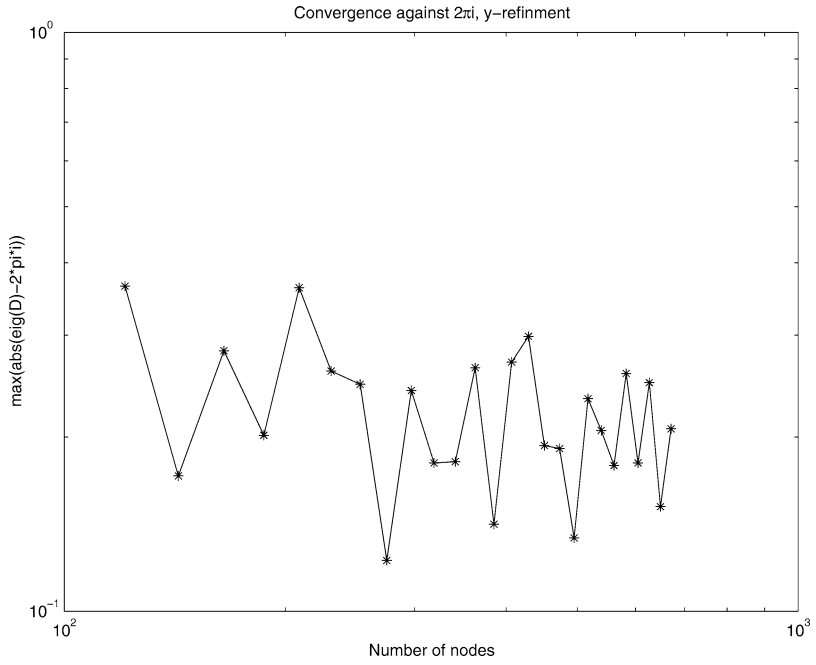

Fig. 14. Convergence against the point $2\pi i$. New nodes are introduced in the y-direction only.

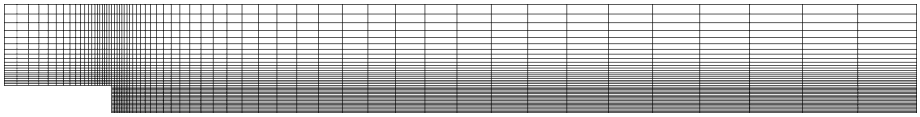

Fig. 15. Mesh for the backward facing step calculation.

(The point 0 was omitted because it is contained in all spectra.) Two cases were tested; the convergence when the new nodes were introduced in the x-direction only, and the convergence when new nodes were introduced in the y-direction only.

Figs. 11–14 show that we have a second order accurate scheme. The refinement in the y-direction does not lead to more accurate solutions since the problem (24) contains x-derivatives only. (In Figs. 11 and 12 two points deviate a lot from the others. The reason for that deviation is degenerated meshes obtained from Matlab.)

3.2. A two-dimensional nonlinear system

In this section we will study the two-dimensional Euler equations and in particular the difference between the weak (penalty) and the strong (injection) form of imposing boundary conditions. We will perform a linear constant coefficient analysis and compare with nonlinear calculations. In the two computational cases below, the boundary is either a solid wall (denoted by $\delta\Omega_S$) or an artificial boundary (denoted $\delta\Omega_A$), see Figs. 15 and 18.

Consider (1) with characteristic boundary conditions at $\delta\Omega_A$ and the solid wall boundary condition $\hat{u}\cdot\hat{n}=0$ at $\delta\Omega_S$. The energy rate before imposing the solid wall boundary condition becomes (see (20))

$$\frac{\mathrm{d}}{\mathrm{d}t}\|u\|^2 = -\int_{\partial\Omega_A}\left[v^{\mathrm{T}}\Lambda^+ v + g^{\mathrm{T}}\Lambda^- g\right]\mathrm{d}s - \int_{\partial\Omega_S}\left[v^{\mathrm{T}}\Lambda v\right]\mathrm{d}s. \tag{39}$$

To evaluate the second term in (39) we must be more specific and introduce the matrix

$$\alpha A+\beta B=\begin{pmatrix} \bar{w}_n & \alpha\bar{c}/\sqrt{\gamma} & \beta\bar{c}/\sqrt{\gamma} & 0\\ \alpha\bar{c}/\sqrt{\gamma} & \bar{w}_n & 0 & \alpha\bar{c}\sqrt{(\gamma-1)/\gamma}\\ \beta\bar{c}/\sqrt{\gamma} & 0 & \bar{w}_n & \beta\bar{c}\sqrt{(\gamma-1)/\gamma}\\ 0 & \alpha\bar{c}\sqrt{(\gamma-1)/\gamma} & \beta\bar{c}\sqrt{(\gamma-1)/\gamma} & \bar{w}_n \end{pmatrix},$$

where $(\alpha,\beta)^{\mathrm{T}}=\hat{n}$ is the outward pointing unit normal, $\hat{t}=(-\beta,\alpha)^{\mathrm{T}}$ the unit tangent vector and A, B are the constant symmetric matrices in the symmetrized Euler equations derived in [4], see also [23]. The dependent variables and parameters $w_n=\hat{u}\cdot\hat{n},\ w_t=\hat{u}\cdot\hat{t},\ c,\ p,\ \rho$ and γ are the component of the velocity normal and tangential to the boundary, the speed of sound, the pressure, the density and the ratio of specific heats, respectively. The over-bar is used to denote a variable at the constant reference state.

The symmetric matrix $\alpha A+\beta B$ can be diagonalised as $X\Lambda X^{\mathrm{T}}$ where

$$\begin{aligned} \Lambda &= \begin{pmatrix} \bar{w}_n-\bar{c} & 0 & 0 & 0\\ 0 & \bar{w}_n & 0 & 0\\ 0 & 0 & \bar{w}_n & 0\\ 0 & 0 & 0 & \bar{w}_n+\bar{c} \end{pmatrix},\\ X^{\mathrm{T}}u = v &= \begin{pmatrix} p-\bar{\rho}\bar{c}w_n\\ \theta(p-\bar{\rho}c^2)\\ w_t\\ p+\bar{\rho}\bar{c}w_n \end{pmatrix}, \end{aligned} \tag{40}$$

and $\theta=\sqrt{2/(\gamma-1)}$. v in (40) are the characteristic variables. The boundary condition $\bar{w}=w=0$ implies that the contribution to the energy rate (39) from the solid wall $\partial\Omega_S$ becomes identically zero since

$$v^{\mathrm{T}}\Lambda v=[\bar{w}_n=0]=-\bar{c}\left(v_1^2-v_4^2\right)=[w_n=0]=0, \tag{41}$$

on $\partial\Omega_S$ by repeated use of (40).

Next, the discrete approximation (13) of (1) with characteristic boundary conditions at $\delta\Omega_A$ and the solid wall boundary condition $\hat{u}\cdot\hat{n}=0$ at $\delta\Omega_S$ is considered. The energy rate (see (23)) with a penalty formulation of the discrete solid wall boundary condition $((v_1-v_4)_i=0)$ included becomes

$$\frac{\mathrm{d}}{\mathrm{d}t}\|\boldsymbol{u}\|^2_{I\otimes P} = -\sum_{\delta\Omega_A}\left[\boldsymbol{v}^{\mathrm{T}}\Lambda^+\boldsymbol{v}+g^{\mathrm{T}}\Lambda^- g\right]_i\Delta s_i + R - \sum_{\delta\Omega_S}\left[\boldsymbol{v}^{\mathrm{T}}(\Lambda\boldsymbol{v}+2b)\right]_i\Delta s_i, \tag{42}$$

where $b_i=(v_1-v_4)_i(\sigma_1,\sigma_2,\sigma_3,\sigma_4)_i^{\mathrm{T}}$. $R\leqslant 0$ is of the form given in the first remark in Section 2.3. Exactly as in the continuous case, the contribution to the energy rate (42) from the solid wall $\partial\Omega_S$ becomes identically zero since

$$\left(\boldsymbol{v}^{\mathrm{T}}(\Lambda\boldsymbol{v}+2b)\right)=[\bar{w}_n=0]=\bar{c}(v_4-v_1)\left((v_4+v_1)\bar{c}+2\sigma_1 v_1+2\sigma_4 v_4\right)=0, \tag{43}$$

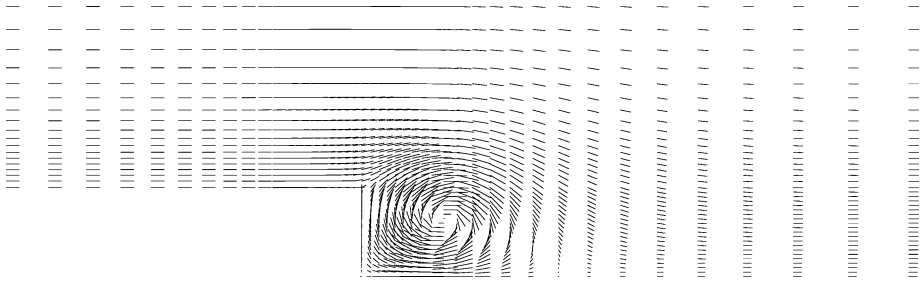

Fig. 16. Velocity distribution in the backward facing step calculation.

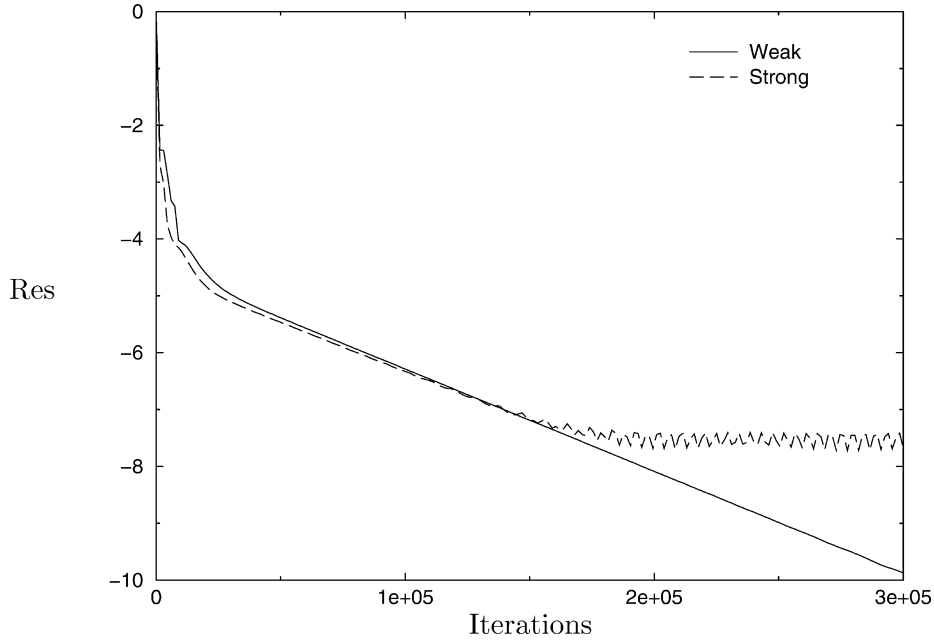

Fig. 17. Convergence history for the backward facing step calculation.

for all $i \in \delta\Omega_S$ and $\sigma_1 = \sigma_4 = -\bar{c}/2$. The values of σ_2, σ_3 are arbitrary.

The estimates (39) and (42) together with the observations (41) and (43) means that the discrete approximation (13) of (1) with characteristic boundary conditions at $\delta\Omega_A$ and the solid wall boundary condition $\hat{u} \cdot \hat{n} = 0$ at $\delta\Omega_S$ is strictly stable in the sense of Definition 1.

To evaluate the relevance of the linear analysis above for nonlinear problems, two computational cases was considered. In the first case, a structured mesh was used to compute the flow over a backward facing step at Mach number 0.2, see Figs. 15, 16. The convergence history for a weak and strong imposition of boundary conditions are shown in Fig. 17. Clearly the strictly stable weak imposition of boundary conditions is superior. The calculation where strong imposition (injection is used) does not converge.

In the second calculation, an unstructured mesh (see Fig. 18) was used to compute the flow over a Naca0012 air-foil at Mach number 0.5. Also in this case, the strictly stable weak imposition of boundary conditions converges while the strong imposition prevents convergence, see Fig. 19. The non-existent

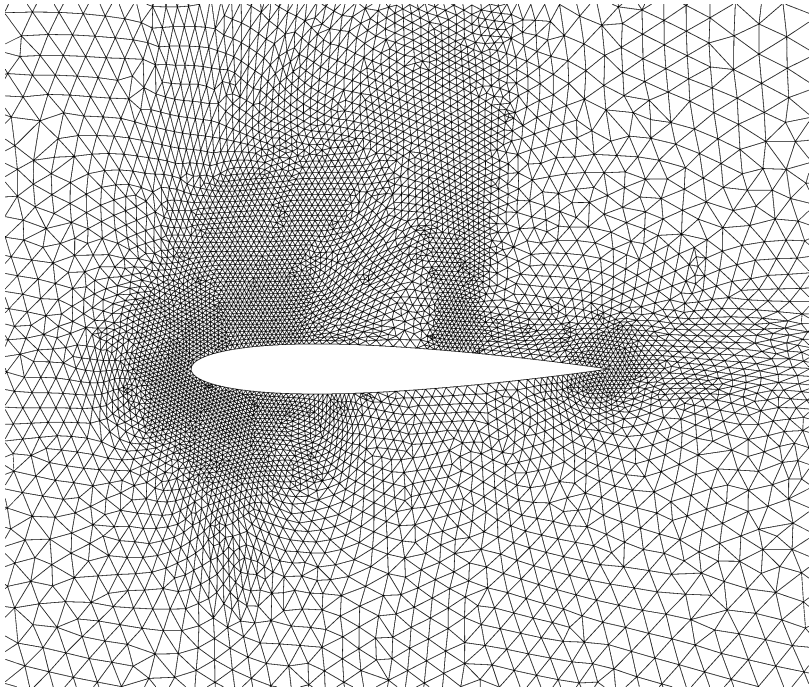

Fig. 18. Mesh for the Naca0012 calculation.

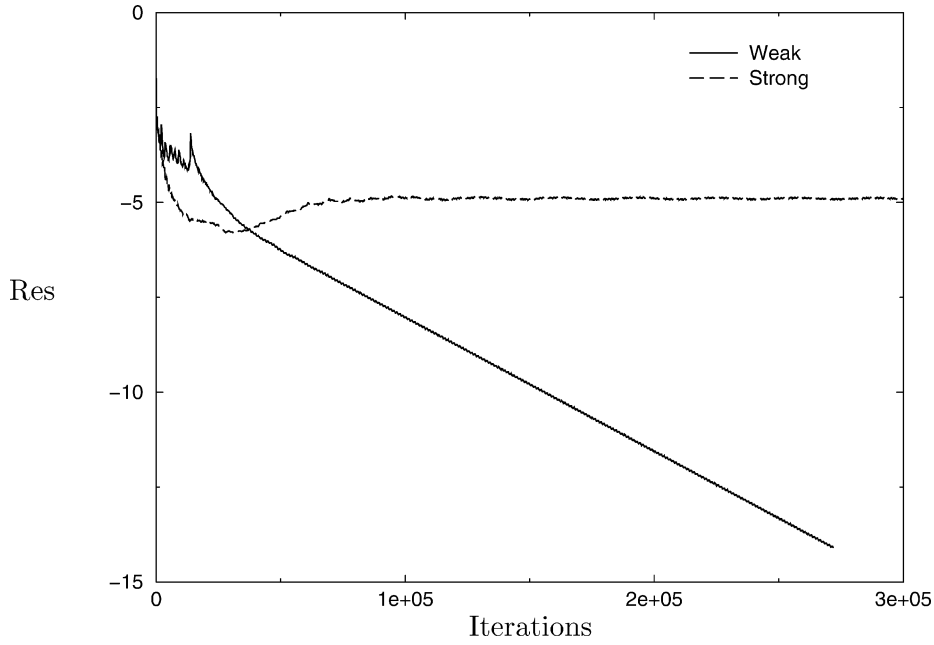

Fig. 19. Convergence history for the Naca0012 calculation.

convergence for the cases where injection was used could possibly be the result of incorrect location of the eigenvalues from the spatial operator, see Section 3.1.1.

4. Conclusions

It has been shown that it is possible to generalize the concept of SBP-operators to node centered finite volume methods on unstructured grids.

To introduce boundary conditions weakly is shown to be equivalent to the standard penalty procedure (SAT) for boundary conditions used together with SBP-operators.

The method analyzed in this work with boundary conditions imposed weakly lead to energy estimates and strict stability if one specifies the ingoing characteristic variable and/or imposes no slip boundary conditions.

Furthermore, the method of injection of boundary conditions does not always lead to energy estimates and sometimes results in an unstable scheme or in calculations that do not converge to steady state.

References

[1] S. Abarbanel, A. Ditkowski, Asymptotically stable fourth-order accurate schemes for the diffusion equation on complex shapes, J. Comput. Phys. 133 (2) (1997) 279–288.
[2] S. Abarbanel, A. Ditkowski, Multi-dimensional asymptotically stable finite difference schemes for the advection–diffusion equation, Comput. Fluids 28 (4–5) (1999) 481–510.
[3] S. Abarbanel, A. Ditkowski, B. Gustafsson, On error bounds of finite difference approximations to partial differential equations—Temporal behavior and rate of convergence, J. Sci. Comput. 15 (1) (2000) 79–116.
[4] S. Abarbanel, D. Gottlieb, Optimal time splitting for two- and three-dimensional Navier–Stokes equations with mixed derivatives, J. Comput. Phys. 41 (1) (1981) 1–33.
[5] M.H. Carpenter, J. Nordström, D. Gottlieb, A stable and conservative interface treatment of arbitrary spatial accuracy, J. Comput. Phys. 148 (1999) 341–365.
[6] M.H. Carpenter, D. Gottlieb, S. Abarbanel, Time-stable boundary conditions for finite-difference schemes solving hyperbolic systems: Methodology and applications to high-order compact schemes, J. Comput. Phys. 111 (1994) 220–236.
[7] P. Eliasson, EDGE a Navier–Stokes solver for unstructured grids, Scientific Report, FOI-R-0298-SE, 2001.
[8] T. Gerhold, J. Evans, Efficient computation of 3d flow for complex configurations with the DLR-TAU code, in: W. Nitsche, H.-J. Heinemann, R. Hilbig (Eds.), in: Notes on Numerical Fluid Mechanics (NNFM), Vol. 72, Vieweg, Braunschweig, 1999.
[9] T. Gerhold, O. Friedrich, J. Evans, M. Galle, Calculation of complex three-dimensional configurations employing the DLR-TAU code, 35th Aerospace Sciences Meeting and Exhibit, AIAA 97-0167, Reno, NV, 1997.
[10] B. Gustafsson, On the implementation of boundary conditions for the method of lines, BIT 38 (2) (1998) 293–314.
[11] B. Gustafsson, H.-O. Kreiss, J. Oliger, Time Dependent Problems and Difference Method, Wiley, New York, 1995.
[12] B. Gustafsson, P. Olsson, Fourth-order difference methods for hyperbolic IBVPs, J. Comput. Phys. 117 (2) (1995) 300–317.
[13] A. Hasselbacher, J.J. McGuirk, G.J. Page, Finite volume discretization aspects for viscous flows on mixed unstructured grids, AIAA J. 37 (2) (1999) 177–184.
[14] A. Jameson, Positive schemes and shock modelling for compressible flows, Internat. J. Numer. Methods Fluids 20 (8–9) (1995) 743–776, Finite elements in fluids—New trends and applications (Barcelona, 1993).
[15] A. Jameson, T.J. Baker, N.P. Weathrill, Calculation of inviscid transonic flow over a complete aircraft, 24th Aerospace Sciences Meeting and Exhibit, AIAA 86-0103, Reno, NV, 1986.

[16] A. Jameson, D. Mavriplis, Finite volume solution of the two-dimensional Euler equations on a regular triangular mesh, 23th Aerospace Sciences Meeting and Exhibit, AIAA 85-0435, Reno, NV, 1985.
[17] H.-O. Kreiss, G. Scherer, Finite element and finite difference methods for hyperbolic partial differential equations, in: C. De Boor (Ed.), Mathematical Aspects of Finite Elements in Partial Differential Equations, Academic Press, New York, 1974.
[18] D.J. Mavriplis, Mesh generation and adaptivity for complex geometries and flows, in: R. Peyret (Ed.), Handbook of Computational Fluid Mechanics, Academic Press, San Diego, CA, 1996, pp. 417–459.
[19] D.J. Mavriplis, Unstructured grid techniques, Annu. Rev. Fluid Mech. 29 (1997) 473–514.
[20] D.J. Mavriplis, Multigrid strategies for viscous flow solvers on anisotropic unstructured meshes, J. Comput. Phys. 145 (1) (1998) 141–165.
[21] D.J. Mavriplis, A three-dimensional multigrid reynolds-averaged Navier–Stokes solver for unstructured meshes, AIAA J. 33 (3) (1995) 445–453.
[22] J. Nordström, M. Björck, Finite volume approximations and strict stability for hyperbolic problems, Appl. Numer. Math. 28 (2001) 237–255.
[23] J. Nordström, The use of characteristic boundary conditions for the Navier–Stokes equations, Comput. Fluids 24 (5) (1995) 609–623.
[24] J. Nordström, M.H. Carpenter, Boundary and interface conditions for high order finite difference methods applied to the Euler and Navier–Stokes equations, J. Comput. Phys. 148 (1999) 621–645.
[25] J. Nordström, M.H. Carpenter, High-order finite difference methods, multidimensional linear problems, and curvilinear coordinates, J. Comput. Phys. 173 (1) (2001) 149–174.
[26] P. Olsson, Summation by parts, projections, and stability, I, Math. Comp. 64 (211) (1995) 1035–1065, S23–S26.
[27] P. Olsson, Summation by parts, projections, and stability, II, Math. Comp. 64 (212) (1995) 1473–1493.
[28] O. Peroomian, S. Chakravarthy, U.C. Goldberg, A "grid-transparent" methodology for CFD, 35th Aerospace Sciences Meeting and Exhibit, AIAA 97-0724, Reno, NV, 1997.
[29] B. Strand, Summation by parts for finite difference approximations for $\mathrm{d}/\mathrm{d}x$, J. Comput. Phys. 110 (1) (1994) 47–67.
[30] B. Strand, Numerical studies of hyperbolic IBVP with high-order finite difference operators satisfying a summation by parts rule, Appl. Numer. Math. 26 (4) (1998) 497–521.
[31] V. Venkatakrishnan, A perspective on unstructured grid flow solver, AIAA J. 34 (3) (1996) 547–553.